

# **Impacts of New Particle Formation on Aerosol Cloud Condensation Nuclei (CCN) Activity in Shanghai: Case Study**

Chunpeng Leng <sup>a</sup>, Qun Zhang <sup>a</sup>, Jun Tao <sup>b</sup>, Hefeng Zhang <sup>c</sup>, Deqin Zhang <sup>a</sup>, Chen Xu <sup>a</sup>, Xiang Li <sup>a</sup>, Lingdong Kong <sup>a</sup>, Tiantao Cheng <sup>a</sup>, Renjian Zhang <sup>d</sup>, Xin Yang <sup>a</sup>, Jianmin Chen <sup>a</sup>, Liping Qiao <sup>e</sup>, Shenrong Lou <sup>e</sup>,  
Hongli Wang <sup>e</sup>, Changhong Chen <sup>e</sup>

a. Shanghai Key Laboratory of Atmospheric Particle Pollution and Prevention (LAP<sup>3</sup>), Fudan-Tyndall Centre, Department of environmental science and engineering, Fudan University, Shanghai 200433, China;

b. South China Institute of Environmental Sciences, Ministry of Environmental Protection, Guangzhou 510655, China;

c. Atmospheric Environment Institute, Chinese Research Academy of Environmental Sciences, Beijing 100012, China;

d. Key Laboratory of Region Climate-Environment Research for Temperate East Asia, Institute of Atmospheric Physics, Chinese Academy of Sciences, Beijing 100029, China;

e. State Environmental Protection Key Laboratory of the Cause and Prevention of Urban Pollution Complex, Shanghai Academy of Environmental Sciences, Shanghai 200233, China;

\* Corresponding authors: Tiantao Cheng; Jianmin Chen

Tel: (86) 21-6564 3230; fax: (86) 21-6564 2080;

Email: [ttcheng@fudan.edu.cn](mailto:ttcheng@fudan.edu.cn), [jmchen@fudan.edu.cn](mailto:jmchen@fudan.edu.cn)

## Abstract

New particle formation (NPF) events and their impacts on cloud condensation nuclei (CCN) were investigated using continuous measurements collected in urban Shanghai from 1 to 30 April 2012. During the campaign, NPF occurred in 8 out of the 30 days and enhanced CCN number concentration ( $N_{\text{CCN}}$ ) by a factor of 1.2-1.8, depending on supersaturation (SS). The NPF event on 3 April 2012 was chosen as an example to investigate the NPF influence on CCN activity. In this NPF event, secondary aerosols were produced continuously and increased  $\text{PM}_{2.5}$  mass concentration at a rate of  $4.33 \mu\text{g cm}^{-3} \text{ h}^{-1}$ , and the growth rate (GR) and formation rate (FR) were on average  $5 \text{ nm h}^{-1}$  and  $0.36 \text{ cm}^{-3} \text{ s}^{-1}$ , respectively. The newly formed particles grew quickly from nucleation mode (10-20 nm) into CCN size range.  $N_{\text{CCN}}$  increased rapidly at SS of 0.4-1.0% but weakly at SS of 0.2%. Correspondingly, aerosol CCN activities (fractions of activated aerosol particles in total aerosols,  $N_{\text{CCN}}/N_{\text{CN}}$ ) were significantly enhanced from 0.24-0.60 to 0.30-0.91 at SS of 0.2-1.0% due to the NPF. On the basis of the  $\kappa$ -Köhler theory, aerosol size distributions and chemical composition measured simultaneously were used to predict  $N_{\text{CCN}}$ . There was a good agreement between the predicted and measured  $N_{\text{CCN}}$  ( $R^2=0.96$ ,  $N_{\text{predicted}}/N_{\text{measured}}=1.04$ ). This study reveals that NPF exerts large impacts on aerosol particle abundance and size spectra, thus significantly promotes  $N_{\text{CCN}}$  and aerosol CCN

activity in this urban environment. The GR of NPF is the key factor controlling the newly formed particles to become CCN at all SS levels, whereas the FR is an effective factor only under high SS (e.g. 1.0%) conditions.

**Key words:** cloud condensation nuclei, new particle formation, particle property, urban

## 1. Introduction

Atmospheric aerosols exert great impacts on global climate by affecting the earth's radiation balance through directly scattering and absorbing solar and terrestrial lights, and indirectly modifying cloud by acting as cloud condensation nuclei (CCN) (Charlson et al., 1992; Lohmann et al., 2005). The indirect effect of primary and secondary aerosols brings up the largest uncertainty to predictions of aerosol radiative forcing and global climate change (IPCC, 2013). So far, many studies of field observation and modeling have found that new particle formation (NPF) significantly impacts aerosols and CCNs at worldwide locations (Ghan et al., 2001; Spracklen et al., 2006, 2008; Zhang, 2010).

Normally, NPF in the atmosphere is identified as the nucleation of gas phase precursors and subsequent condensational growth, which is a crucial secondary transformation course (Birmili et al., 2000; Kulmala et al., 2004). In fact, NPF consists of a complex set of procedures, including

the formation of nanometer-size clusters from gaseous vapors, the growth of these clusters, the removal of growing clusters by coagulation with pre-existing particles, and the further growth of survived clusters into aerosol particles, some of which are large enough to become CCN (McMurry et al., 1983, 2005; Weber et al., 1996). The NPF event can be effectively characterized by the formation rate (FR) of nucleation mode particles and the growth rate (GR) of freshly nucleated particles (Kulmala et al., 2012). On the basis of over 100 field measurements summarized by Wang et al. (2013), significant gaps still exist regarding both formation and growth rate outputs. For example, the GR varied in the range of 1-20 nm h<sup>-1</sup> and the FR in 0.01-10 cm<sup>-3</sup> s<sup>-1</sup>. Condensable gaseous precursors and their coagulation sink responsible for NPF are commonly high in megacities of developing countries (Mönkkönen et al., 2005; Wu et al., 2007). Gaseous sulfur is proved to play a vital role in nucleation process (Petäjä et al., 2009; Kulmala et al., 2013). Atmospheric ammonia can effectively lower the surface pressure of gaseous sulfuric molecular and participates homogeneous nucleation with gaseous sulfuric acid and water vapor (Smith et al., 2004; Sakurai et al., 2005; Gaydos et al., 2005). In addition, there are other species responsible for NPF such as amines (Yu et al., 2012; Benson et al., 2011), low-volatile organic vapors (Metzger et al., 2010; Paasonen et al., 2010; Riipinen et al., 2011; Ehn et al., 2014) and iodine compounds (O'Dowd et al., 2002; Vuollekoski et al., 2009).

The newly formed particles from atmospheric nucleation are often able to grow into CCN size and further influence cloud properties or even global climate (Kerminen et al., 2005; Laaksonen et al., 2005; Wiedensohler et al., 2009). Kerminen et al. (2012) presents a synthesis of our current (by the end of 2012) knowledge of CCN production associated with atmospheric nucleation, and concludes that CCN production associated with atmospheric nucleation is both frequent and widespread phenomenon in numerous types of continental boundary layers, and probably also for a large fraction of the free troposphere. The latest model results show that the NPF events contribute much more to global aerosol number burden than primary emissions (Merikanto et al., 2009; Yu et al., 2008). Under numerous atmospheric conditions aerosol has a positive feedback to CCN number concentration ( $N_{\text{CCN}}$ ) (Ramanathan et al., 2001; Laaksonen et al., 2005), and  $N_{\text{CCN}}$  usually exhibits a significant increase after NPF (O'Dowd et al., 2001; Lihavainen et al., 2003; Kuwata et al., 2008; Yue et al., 2011). Due to various chemical species involved in NPF, the extent of NPF effects on CCN varied temporarily and spatially (Spracklen et al., 2008; Pierce and Adams, 2009). The long-term NPF observations were mainly conducted in Europe and North America, whereas little has been done in developing countries (Wang et al., 2013). To date, only a few studies have concerned NPF and its interaction with CCN in China. Yue et al. (2011) reported

that the GR of sulfur-poor NPF was on average about 80% larger than that of sulfur-rich NPF, and the NPF events increased CCN by 0.4-6 times in Beijing, where various source apportionment of PM<sub>2.5</sub> was reported by Zhang et al. (2013). Wiedensohler et al. (2009) found that the CCN size distribution is dominated by the growing nucleation mode in Beijing, which accounted up to 80% of the total CCN number concentration, in contrast to the usually found phenomenon of the dominance by the accumulation mode.

In the present study, we analyze a comprehensive dataset of 1-month simultaneous measurements of aerosol size spectra, N<sub>CCN</sub>, black carbon (BC), water-soluble ions and gaseous pollutants to understand the NPF events and their impacts on N<sub>CCN</sub> and aerosol CCN activity in an urban environment of Shanghai, one of the largest cities in China. A closure study between predicted and measured CCNs is also conducted to investigate the influence of aerosol chemical composition on its growth to CCN. An effective CCN prediction model is further developed based on model-measurement comparison results.

## **2. Experimental**

### **2.1 Observational site**

All instruments were mounted on the roof of one building approximately 20m above the ground in the campus of Fudan University (31°18'N, 121°29'E) located in Shanghai. The observational site is

mainly surrounded by urban residential areas, where no large local emission was detected during this study. The East China Sea is approximate 40 km east of the site. Except CCN, other measurements conducted synchronously, including aerosol number size distribution (condensation nuclei (CN) of 10-800 nm), major inorganic water-soluble ions in aerosol particles, gaseous pollutants and meteorological factors. Local time (LT) used in this study is eight hours ahead of UTC.

## **2.2 Measurement and instrumentation**

A CCN counter (CCN-100, DMT, USA) with continuous flow and single column (Roberts and Nenes, 2006; Lance et al., 2006) was employed to monitor CCN concentrations at supersaturated conditions (SS in the range of 0.07-2%). Before the campaign, the instrument was calibrated for SS using standard  $(\text{NH}_4)_2\text{SO}_4$  particles. To maintain stable SS, according to the instrument operation manual, regular calibrations were also performed for temperature gradient, input and shear airflows and pressure (Leng et al., 2013). In addition, periodic zero checks were done to ensure counting accuracy for optical particle counter (OPC) installed inside the CCN counter. The ambient aerosol was firstly dried by a dryer (active carbon) to lower relative humidity (RH) below 30%, and subsequently introduced into the CCN counter (Leng et al., 2013).

Aerosol particle size distributions in the size range of 10-800 nm were measured using a high-resolution scanning mobility particle sizer (SMPS,

TSI 3080, USA). Before and after the field campaign, the instrument was calibrated to maintain accurate particle sizing. The SMPS data are recorded by AIM (Aerosol Instrument Management) software from TSI company. The SMPS 3936 (TSI corp.) is employed to track the size distribution change, in which the CPC 3736 (TSI corp.) is used to count the number of particle of each size. The neutralizer 3077a (TSI corp.) is used in the system to provide known charge on the particles going into the SMPS. The size of the employed impactor is 0.071 cm. Both multiple charge and the diffusion correction is applied. The inlet information has been reported in our previously papers (Wang et al., 2009; Huang et al., 2013).

BC was measured by an online monitor of Aethalometer (AE-31, Magee Scientific Co., Berkeley, California, USA) at a 5-min time resolution and a 5 l/min airflow rate. According to the strong ability of BC light absorption at near infrared wavelengths (Hansen et al., 1984; Weingartner et al., 2003), BC mass is determined using the light attenuation at 880 nm and the appropriate specific attenuation cross section proportional to BC (Petzold et al., 1997). The attenuation can be calculated based on the intensity difference of reference and sensing beams between light on and off (Dumka et al., 2010). In order to screen the impacts of other absorptive material, the data contaminated by mineral and dust aerosols were excluded from BC measurements. Details



for instrument operating and calibrating can be found in Cheng et al. (2010).

A monitor of aerosols and gases (MARGA, ADI 2080, Netherlands) was employed to measure the mass concentrations of major inorganic water-soluble ions ( $\text{Na}^+$ ,  $\text{K}^+$ ,  $\text{Mg}^+$ ,  $\text{Ca}^+$ ,  $\text{SO}_4^{2-}$ ,  $\text{Cl}^-$ ,  $\text{NO}_3^-$  and  $\text{NH}_4^+$ ) in ambient aerosol particles at a 1h time resolution. The methods of sampling, operation and internal calibration of the MARGA were described in Du et al. (2011).

A continuous ambient particulate monitor (FH62C14, Thermo) was used to measure  $\text{PM}_{2.5}$  (particles in aerodynamic diameter less than 2.5  $\mu\text{m}$ ) concentration online. The Thermo FH62C14 Continuous Ambient Particulate Monitor (FH62C14) is a radiometric particulate mass monitor capable of providing real-time measurements. It incorporates time-averaged measurements of an integral beta attenuation sensor and advanced firmware to optimize the continuous mass measurement. The FH62C14 equips a dynamic heating system (DHS) to maintain the relative humidity (RH) of the air passing through the filter tape of the radiometric stage well below the point at which the collected particles accrete and retain liquid water. The DHS system minimizes the internal temperature rise ensuring negligible loss of semi-volatiles from the collected sample when the ambient RH is below the threshold to which the heater is controlling. As the ambient RH increases above the threshold,

the applied heating is optimized to maintain the RH threshold above the beta attenuation filter tape. Necessary sensor calibrations are performed for temperature, relative humidity, barometric pressure and volumetric flow regularly to maintain valid measurements.

Moreover, an automatic weather station client (HydroMet<sup>TM</sup>, Vaisala) and a visibility monitor (Belford, M6000) were employed to collect the data of meteorological variables and atmospheric visibility.

### 3. Results and discussion

#### 3.1 Overview of the entire period

The ground-based measurements contained  $N_{CCN}$  at SS of 0.2-1.0%, aerosol size spectra, atmospheric visibility,  $PM_{2.5}$ , BC, aerosol inorganic water-soluble ions and  $SO_2$  and were conducted during the period of 1-30 April 2012. Figure 1 describes the general meteorological conditions (e.g. wind speed, wind direction, RH and temperature) for the entire period. Wind frequently changed direction and were mostly weaker than  $6 \text{ m s}^{-1}$ . There was no significant precipitation in this month and RH seldom exceeded 90%. Temperature generally varied between 10-25 °C.

Figure 2 shows the temporal variations of 5-min mean  $SO_2$ ,  $PM_{2.5}$  concentration and atmospheric visibility for the entire period. In general,  $PM_{2.5}$  and visibility were negatively correlated and averaged  $70 \pm 60 \mu\text{g m}^{-3}$  and  $24.3 \pm 23.7 \text{ km}$ , respectively. The maximum and average of  $PM_{2.5}$  in the current study is of less magnitude than those measured in a

previous study in 2006 in this urban environment which showed a range of 17.8-217.9  $\mu\text{g m}^{-3}$  and an average of 94.6  $\mu\text{g m}^{-3}$  (Wang et al., 2006).  $\text{PM}_{2.5}$  frequently experienced a clear inter-day oscillating with a similar intra-day cycle.  $\text{PM}_{2.5}$  can reflect the variations of ambient particulate pollutant loadings in the boundary atmosphere layer, and can be viewed as an additional proxy of pre-existing particle amounts for identifying NPF. In a broad view, atmospheric visibility frequently declined to be less than 10 km, revealing heavily polluted episode occurrences (e.g. haze). In fact, the haze or hazy days accounted for 50% of the study period, during which atmospheric visibility was on average 5.65 km, while it was 24.3 km on average for the rest of the days.

### **3.1.1 New particle formation event**

It has been widely accepted that the key criterion for discerning an NPF event is to identify an acute burst of nucleation mode particles, known as newly formed particles up to detectable size of 3 nm exceeding the background level and lasting for several hours and subsequent growth in mean particle size (Birmili and Wiedensohler, 2000; Kulmala et al., 2004, 2012; Vakkari et al., 2011). The supplementary criteria are also needed for identifying NPF, such as low pre-existing particle loading, an apparent “banana” shaped particle number concentration as a function of time and size, and favorable weather conditions essential for excluding pre-existing particle disturbance particularly in urban environment (Shi et

al., 2001; Heintzenberg et al., 2007; Olofson et al., 2009). In this study, although the SMPS is only capable of capturing particles no less than 10 nm, the aerosol size spectra from the SMPS measurements was available to determine NPF and to calculate the FR and GR of NPF.

In this study, the days with distinct bursts of nucleation mode (10-20 nm) particles lasting for at least 1.5 h from their initial outbreak to maximum in number concentration, and with apparent growth to larger sizes (e.g. 20-50 nm) for a few hours, were defined as effective NPF days. The rest of the days were defined as non-NPF days. Figure 3 shows the 1-month series of aerosol size distribution, 4-min mean total ( $N_{\text{total}}$ ) and nucleation mode ( $N_{10-20\text{nm}}$ ) aerosol number concentration and 1 h mean CCN concentration. On a whole, 8 out of the 30 days were characterized as the NPF days, which represented an occurrence frequency of 27% and was much higher than the 5.4% measured by Du et al (2012) at the same site in winter. Many studies have observed greater NPF frequency in springtime in northern hemisphere. For example, seasonal NPF pattern with a spring maximum and winter minimum is typical for all Nordic stations (Dal Maso et al., 2007; Kristensson et al., 2008; Vehkamäki et al., 2004). In North China Plain, The number of events was highest in the spring months (Wang et al., 2013). The high frequency during spring in urban Shanghai is probably due to high frequency of strong wind from northern China, which helps removing the pre-existing particles in the

atmosphere and further favors the occurrence of new particle formation events (Wu et al., 2008; Wang et al., 2013).

### **3.1.2 Formation and growth rate, and condensation sink**

Formation and growth rates are two essential factors characterizing NPF events (Yue et al., 2011; Kulmala et al., 2012). The FR rate is theoretically defined as the mean increase rate of nucleation mode particle in number concentration as a function of time ( $dN_{\text{nucleation}}/dt$ ) during the nucleation stage of a NPF event. In this paper, due to the losses of newly-formed nucleated particles caused by coagulation, and the measurement unavailable for 3-10 nm particles, this calculation only yielded an “apparent particle formation rate (APFR)” (Du et al., 2012). It should be noted that this APFR would be an underestimate in comparison with the actual formation rate. On the other hand, the GR rate refers to the mean size growing rate of nucleated particles in geometric mean diameter as a function of time during the growth stage of a NPF event, which has been described in details elsewhere (Kulmala et al., 2001, 2004b; Dal Masol et al., 2005). The mode diameter, namely a calibrated geometric mean diameter automatically made by SMPS itself for all aerosol size bins instead of only for nucleated particles, is used to calculate particle growth rate in this study. Similarly, this calculation produces an “apparent particle growth rate (APGR)”. The APGR would be an overestimate in comparison with the real growth rate due to inclusion of the GR rate

caused by coagulation, which is not related to particle mass increases (Kerminen and Kulmala., 2002).

The condensation sink (CS) describes how rapidly vapor molecules can condense onto the particles and can be used to represent the pre-existing particle concentrations (Kulmala et al., 2001). Its values can be directly calculated from the measured aerosol particle size distributions using equation (1) as following:

$$CS = 2\pi D \sum \beta D_p N \quad (1)$$

Where  $D$  is the diffusion coefficient of the condensing vapor,  $\beta$  is the transitional regime correction factor and can be determined using method from Fuchs and Sutugin (1971),  $D_p$  is the particle diameter and  $N$  is the particle number concentration of corresponding size. More explanations and the derivation process for equation (1) can be seen in many studies (Kulmala et al., 2001, 2005; Dal Maso et al., 2002, 2005; Gong et al., 2010; Shen et al., 2011; Gao et al., 2012; Wang et al., 2013), therefore it was only briefly summarized here. It is worth noting that this calculated CS might be underestimated compared to the real values because its derivation is based on the dry particle number size distributions incapable of necessarily representing ambient wet condition well in this study. The uncertainty coming from the effect of ambient hygroscopic growth of aerosols on CS ranges from 5% to 50% (Kulmala et al., 2001).

The mean formation and growth rates of NPF events were  $0.40 \text{ cm}^{-3} \text{ s}^{-1}$

and  $4.91 \text{ nm h}^{-1}$ , respectively, during the whole campaign. The formation and growth rates showed a strong location dependence, for example, higher formation and growth rates have been observed in New Delhi ( $3.3\text{-}13.9 \text{ cm}^{-3} \text{ s}^{-1}$ ,  $11.6\text{-}18.1 \text{ nm h}^{-1}$ ) and Atlanta ( $20\text{-}70 \text{ cm}^{-3} \text{ s}^{-1}$ ), while comparable values were measured in Beijing ( $6 \text{ cm}^{-3} \text{ s}^{-1}$ ,  $4 \text{ nm h}^{-1}$ ) for sulfur-rich aerosol type and ( $2 \text{ cm}^{-3} \text{ s}^{-1}$ ,  $6 \text{ nm h}^{-1}$ ) for sulfur-poor aerosol type and in Shanghai ( $3.3\text{-}5.5 \text{ nm h}^{-1}$ ) (Kulmala et al., 2004; Mönkkönen et al., 2005; Yue et al., 2011; Du et al., 2012). The mean CS values were  $0.021 \text{ s}^{-1}$  on the NPF event days and  $0.040 \text{ s}^{-1}$  on the non-event days, lower than those measured in Beijing ( $0.027 \pm 0.021$  and  $0.047 \pm 0.024 \text{ s}^{-1}$ ) and New Delhi ( $0.050\text{-}0.070 \text{ s}^{-1}$ ), and higher than those observed in Shangdianzi (SDZ, a regional station located in the North China Plain, about 120 km northeast of Beijing,  $0.020 \pm 0.020$  and  $0.026 \pm 0.018 \text{ s}^{-1}$ ), and European urban environments including Marseille ( $0.003\text{-}0.015 \text{ s}^{-1}$ ), Athens ( $0.006\text{-}0.013 \text{ s}^{-1}$ ) and Helsinki ( $0.006 \text{ s}^{-1}$ ) (Kumala et al., 2005; Hussein et al., 2008; Wang et al., 2013).

### 3.1.3 NPF impacts on aerosol CCN activity

Pierce and Adams (2007) are the first ones that present the full theoretical framework on the efficiency of CCN production resulting from nucleation. To explore the NPF potential influence on CCN, we further examined the impacts of FR and GR rates in NPF events on  $N_{\text{CCN}}$  and aerosol CCN activity. Table 1 summarizes the  $N_{\text{CCN}}$  enhancement

ratios for different FR and GR levels during the entire campaign.

It has been widely recognized that  $N_{CCN}$  is positively correlated to  $N_{CN}$  under various atmospheric conditions (Ramanathan et al., 2001; Laaksonen et al., 2005), and enhancements on  $N_{CCN}$  are expected after NPF events (O'Dowd et al., 2001; Kuang et al., 2009; Yue et al., 2011). Theoretically, the high FR rate produces more secondary aerosol particles (i.e.  $N_{CN}$ ), which may subsequently impact  $N_{CCN}$  if new particles grow into greater sizes (Ghan et al., 2001; Spracklen et al., 2006, 2008; Zhang, 2010). In this paper, however,  $N_{CCN}$  was insensitive to the FR rate of NPF at SS of 0.2-0.8%, as indicated by the small differences in  $N_{CCN}$  enhancement ratios under various FR and SS values. This finding agrees with the results of earlier studies that the nucleation of newly formed particles within the boundary layer poses a minor impact on  $N_{CCN}$ . Carslaw et al. (2007) found that  $N_{CCN}$  increased only by 12-17% after a two order of magnitude increase of nucleation rate in central Europe. A similar result has been reported in Beijing (Yue et al., 2011). The possible explanation is in two aspects. The first one is due to the two separate and self-governed processes in particle formation and subsequent growth. A high formation rate does not necessarily correspond to a high GR rate since the newly formed particles may not grow into CCN size with insufficient time period. The second one is due to coagulation process between particles which leads to reduced  $N_{CN}$  and further lowers  $N_{CCN}$ .



enhancement ratios. In fact, the impact of FR in NPF on  $N_{CCN}$  enhancement increased with SS (Table 1). The lower critical dry diameter under higher SS for a given aerosol particle was probably the main reason. For example, according to the  $\kappa$ -Köhler theory (Köhler., 1936; Petters and Kreidenweis., 2007), pure NaCl particles can act as CCN only at 65 nm under SS 0.2%, while it can be activated at 22 nm under SS 1.0%. Presumably, with the presence of an unrealistic high SS where all nucleation mode particles (10-20 nm) are activated, the formation rate would be one controlling factor.

On the other hand, what controls a newly formed particle to become a CCN is its survival probability whether it has enough time to grow into thermodynamic stable size by competing with the capture and removal of pre-existing particles (Kerminen et al., 2001; Pierce and Adams, 2007; Zhang et al., 2012). Toward to this end, the aerosol GR rate of NPF responsible for this survival probability was observed to exert a valid effect on  $N_{CCN}$  enhancement ratios. As was found in this study, the  $N_{CCN}$  enhancement ratios at larger GR rate were higher than those at lower GR rate by a factor of 1.06-1.13 depending on SS.

Overall, the  $N_{CCN}$  enhancement ratios due to NPF varied as a function of FR and GR rates and SS. In real atmosphere, SS varies from exceeding 1.0% in clean-air stratus cloud to slightly less than 0.1% in polluted conditions (Hudson and Noble, 2014). FR may logically play a vital role

in CCN production in the clean-air stratus cloud while exert a minor impact in polluted conditions. GR is invariably the most important factor in controlling the extent of newly formed particles in becoming CCN during NPF.

## **3.2 Characteristics of the typical NPF**

### **3.2.1 Enhancement of nanoparticles**

The NPF event spanning the period from 10:00 LT on 3 April to 4:00 LT on 4 April is analyzed in detail to shed some light on the relationship between NPF and CCN. This NPF event was identified to consist a nucleation stage (10:00-13:00 LT) and a growth (13:00-4:00 LT) stage (Fig. 4).

Before 10:00 LT on 3 April,  $\text{PM}_{2.5}$  was below  $20 \mu\text{g m}^{-3}$  due to the relatively strong wind speed (e.g.  $6 \text{ m s}^{-1}$ ) favoring pollutant dispersion. BC was less than  $1 \mu\text{g m}^{-3}$  and atmospheric visibility exceeded 30 km (Fig. 5 and 6). Apparently, the pre-existing particles of nucleation mode (10-20 nm) were low (Fig. 7). Newly formed particles increased quickly in just 1.5 hours from the initial outbreak to the maximum concentration of  $1800 \text{ cm}^{-3}$  (Fig. 7). During the same time period,  $N_{\text{CN}}$  increased from 15,000 to 25,000  $\text{cm}^{-3}$ . The newly formed particles grew in size in the following periods (the growth stage) due to condensation, heterogeneous reactions of chemical compounds and coagulation between particles (Wang et al., 2010). The temporal variations of median, geometric mean

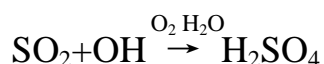
and mode diameters for the measured aerosol population are given in Fig. 7. In general, these three diameters were strongly correlated with each other and increased in size ever since the nucleation burst occurred. During this period, the wind speed was mostly less than  $2 \text{ m s}^{-1}$ , implying a weak atmospheric dilution of pollutants.  $\text{PM}_{2.5}$  increased after 17:00 LT on 3 April, showing a significant enhancement from 38 to  $86 \mu\text{g m}^{-3}$ . In addition, BC correlated well with  $\text{PM}_{2.5}$ , and they both reduce atmospheric visibility.

### 3.2.2 Insights into chemical species involved

Several factors likely determine if a chemical species is to act as nucleation precursor, including its abundance, reactivity and volatility (Zhang et al., 2012). Gaseous  $\text{H}_2\text{SO}_4$  has been proved to be a key precursor participating in nucleation process due to its low volatility (Petäjä et al., 2009; Kulmala et al., 2013), and a necessary condition for new particle formation is for its molecular concentration exceeding  $10^5 \text{ cm}^{-3}$  in atmosphere (Weber et al., 1999, Nieminen et al., 2009). The condensation of gaseous  $\text{H}_2\text{SO}_4$  together with subsequent neutralization with ammonia plays a dominant role in the growth of Aitken mode particles, whereas it exerts little contribution to the growth of particles in accumulation mode (Zheng et al., 2011).

However, direct measurement of sulfuric acid in ambient air is still challenging, appropriate proxies are needed. Petäjä et al. (2009)

measured the sulfuric acid and OH concentration in a boreal forest site in Finland and successfully developed three reasonable proxies for sulfuric acid concentration by using the measured time series as a foundation. Their proxies refer to source (i.e. gaseous SO<sub>2</sub>, hydroxyl radical, solar radiation in 280-320 nm range, and global radiation) and sink (i.e. condensation sink) terms, and the simplest one is the radiation times SO<sub>2</sub> divided by condensation sink. In this paper, the source and radiation terms are unavailable, one may plausibly conjecture similar promotion of H<sub>2</sub>SO<sub>4</sub> on the basis of its gaseous precursor (e.g. SO<sub>2</sub>) evolution (Zhang et al., 2012).



The particle nucleation event showed a burst of 10-20 nm particles when SO<sub>2</sub> peaked at 10:00 LT on 3 April, with its mass and molar concentrations exceeding 4.1 µg m<sup>-3</sup> and 3.8 × 10<sup>10</sup> cm<sup>-3</sup>, respectively (Fig. 8). Afterwards, SO<sub>2</sub> underwent a gradual decrease down to 1.5 µg m<sup>-3</sup>, and SO<sub>4</sub><sup>2-</sup> correspondingly increased from 8 to 10 µg m<sup>-3</sup>. The good agreement between SO<sub>2</sub> and nucleation mode particles denotes the key role of gaseous sulfur in controlling particle nucleation (Zhang et al., 2012; Kulmala et al., 2013).

Besides gaseous sulfur, other nucleation precursors have been proposed to involve in the critical nucleus formation in numerous environment conditions (Riipinen et al., 2011; Zhang et al., 2012). For example,

atmospheric ammonia can significantly lower the surface vapor pressure of gaseous sulfuric acid molecular and participate homogeneous nucleation with gaseous sulfur acid and water vapor. According to the classical ternary homogeneous theory developed recently, the presence of ammonia in ppt level significantly enhances nucleation rates (Yu et al., 2006). Many field measurements and laboratory simulations have corroborated the crucial role of ammonia in the growth of newly formed particles (Smith et al., 2004; Sakurai et al., 2005; Gaydos et al., 2005). Though experimental evidence seems very limited, nitrate has been reported as a crucial contributor to nanoparticle growth, especially for 10-30 nm particles where nitrate is dominant (Hildebrandt et al., 2012). Riipinen et al. (2011) combined observations from two continental sites to show that condensation of organic vapors (i.e. non-volatile and semi-volatile species) is a crucial factor governing the lifetimes and climatic importance of the smallest atmospheric particles. Ehn et al. (2014) find that several biogenic VOCs (e.g. monoterpenes) form large amounts of extremely low-volatility vapours and further demonstrate that these low-volatility vapours can enhance (or even dominate) the formation and growth of aerosol particles over forested regions. In this paper,  $\text{NO}_3^-$  increased by a factor of 1.33 and  $\text{NH}_4^+$  increased by a factor of 1.45 during the case NPF event, indicating that the particle growth is partly driven by the condensation of atmospheric precursors (Fig. 8).

### 3.2.3 Aerosol CCN activity enhancement

Figure 9 shows the temporal evolutions of  $N_{CCN}$  and aerosol CCN activity at SS of 0.2-1.0% for the entire period. The enhanced  $N_{CN}$  and reduced aerosol CCN activity, associated with nucleation mode particle burst, was observed between 10:00 and 13:00 LT on 3 April. In contrast to  $N_{CN}$  which increased immediately after the burst of nucleation mode particles, there was a 4 h delay in the increase of  $N_{CCN}$ . As the newly formed particles grew into larger sizes, both  $N_{CCN}$  and aerosol CCN activity increased at various stages under different SS. At a SS higher than 0.4%,  $N_{CCN}$  peaked at 20:00 LT on 3 April.  $N_{CCN}$  greatly promoted from 8000-12,000  $\text{cm}^{-3}$  to 13,000-20,000  $\text{cm}^{-3}$  under higher SS, however, only slightly from 6000 to 7000  $\text{cm}^{-3}$  under lower SS (e.g. 0.2%). Larger critical dry diameter corresponding to lower SS should be the main reason. For example, the critical dry diameter for pure  $(\text{NH}_4)_2\text{SO}_4$  particle was 83 nm at SS of 0.2% and was only 29 nm at SS of 1.0%. The newly formed particles rarely grew larger than 83 nm in size in this NPF event, hence less  $N_{CCN}$  enhancement was expected at SS of 0.2%. In summary, the  $N_{CCN}$  enhancement ratios were 1.17-1.88 depending on SS value. In Beijing, a larger  $N_{CCN}$  enhancement ratio of 1.4-7 was observed under SS of 0.07-0.86% caused by NPF (Yue et al., 2011).

In comparison with  $N_{CCN}$ , aerosol CCN activity was more sensitive to aerosol size spectra and meteorology factors, which exerts a big

complexity into the temporal variation of aerosol activation. Aerosol activities were effectively reduced by abundant ultra-fine aerosol particles (CCN-inert) produced during the nucleation period. The minimum (0.2-0.6) of aerosol activities was found at 13:00 LT on April when the particle growth started. Owing to the high survival probability of particles growing from nucleation mode to accumulation mode (CCN size), aerosol activities began to increase at different steps for varying SS and reached their maximums of 0.3-0.9 (0.2-1.0% SS) at 4:00 LT on 4 April, eight hours after  $N_{CCN}$  peaked.

#### 3.2.4 Towards CCN closure for NPF

A kappa value  $\kappa$  describing particle hygroscopicity, firstly introduced by Petters and Kreidenweis (2007), was employed here to get CCN closure study during NPF. Assuming aerosol particle population is totally internal-mixed, the effective integrated  $\kappa$  can be obtained through weighting their chemical compound volume fractions,

$$\kappa = \sum_i \varepsilon_i \kappa_i \quad (2)$$

where  $\varepsilon_i$  is the volume fraction of chemical compounds in particles, and  $\kappa_i$  is the effective  $\kappa$  of individual chemical composition. This equation has been widely used and described in detail elsewhere (Petters and Kreidenweis., 2008; Yue et al., 2011). Aerosol particle compositions were classified into three categories, and  $\kappa_i$  and  $\varepsilon_i$  for individual composition are listed in Table 2, of which “others” refers to

PM<sub>2.5</sub>-(SO<sub>4</sub><sup>2-</sup>+NO<sub>3</sub><sup>-</sup>+NH<sub>4</sub><sup>+</sup>+Cl<sup>-</sup>+Na<sup>+</sup>), and is viewed as a chemical compound with  $\kappa_i=0$  (Yue et al., 2011). Due to MARGA data limitations, we only attempted to get CCN closure for the case NPF event in this study. The hourly mean  $\kappa$  values were varying from 0.19 to 0.42, and had an average of 0.28 during the case NPF event. In total, 83.2% of the effective  $\kappa$  was explained by SO<sub>4</sub><sup>2-</sup>+NO<sub>3</sub><sup>-</sup>+NH<sub>4</sub><sup>+</sup>, with their individual contributions of 37.4%, 27.5% and 18.3%, respectively. By using the calculated  $\kappa$ , the critical dry diameter for a particle to act as CCN at a given SS can be determined from an extended  $\kappa$ -Köhler theory:

$$S(D)=\frac{D^3-D_d^3}{D^3-D_d^3(1-\kappa)}\exp(\frac{4\sigma_{s/a}M_w}{RT\rho_w D}) \quad (3)$$

where  $\rho_w$  is the density of water,  $M_w$  is the molecular weight of water,  $\sigma_{s/a}$  is the surface tension of the solution/air interface,  $R$  is the universal gas constant,  $\kappa$  is the hygroscopicity parameter,  $T$  is temperature,  $D$  is the diameter of the droplet and  $S(D)$  is the critical dry size under a given SS. More explanation and the derivation process of equation (3) have been given in detail by Petters and Kreidenweis (2007), therefore there is only brief summarization here. The CCN population can be effectively viewed as a subset of measured aerosol size distributions since the operating range includes the majority of atmospheric particles (10-800 nm). Computed for  $\sigma_{s/a}=0.072$  J m<sup>-2</sup> and  $T=298.15$  K, the predicted CCN number concentration can be calculated through integration between the bottom and top critical dry diameters (i.e.  $S(D)$ ).



Figure 10 provides correlation analysis for the hourly-averaged ( $N=90$ ) predicted and measured  $N_{CCN}$  at SS of 0.2-1.0%. The agreement was excellent between the predicted and measured  $N_{CCN}$ , and a linear regression produced a slope of 0.98 and an intercept of  $-150 \text{ cm}^{-3}$ , with a correlation coefficient ( $R^2$ ) of 0.96. The ratio of  $N_{\text{predicted}}/N_{\text{measured}}$  varied between 0.83 and 1.28 with an average of 1.04.

#### 4. Conclusions

The new particle formation (NPF) events and their impacts on the abundance and properties of cloud condensation nuclei (CCN) were investigated using 1-month continuous measurements collected in downtown Shanghai from 1 to 30 April 2012. The NPF events were observed in 8 out of the 30 days, and their formation and growth rates were  $0.40 \text{ cm}^{-3} \text{ s}^{-1}$  and  $4.91 \text{ nm h}^{-1}$  on average, respectively. The growth rate is important in controlling the conversion of newly formed particles in NPF to possible CCN, whereas the formation rate is viewed as an effective factor only at higher SS (e.g. 1.0%). This is due to the small critical dry diameters for particles to act as CCN under high SS conditions.

The NPF event on 3 April 2012 showed that aerosol particle enhancement in number concentration significantly relates to the length of nucleation period of NPF, and aerosol particle enhancement in mass concentration depends on the growth period. The nucleation period leads

to increased  $N_{\text{CN}}$  and reduced aerosol activity, while the increases in  $N_{\text{CCN}}$  and aerosol activity occurred during the growth period. The newly formed particles needed enough time to grow into CCN size and thus  $N_{\text{CCN}}$  had a delayed peak compared to  $N_{\text{CN}}$ .

Closure between the measured and predicted  $N_{\text{CCN}}$  is successful during the NPF event ( $R^2=0.96$ ).  $\text{SO}_4^{2-}+\text{NO}_3^-+\text{NH}_4^+$  explained the majority of the effective  $\kappa$ , and minimized the impact of lacking organic matter. An overestimation of 4% for  $N_{\text{CCN}}$  is probably introduced by the following uncertainties: (1) aerosol assumed to be completely internal-mixed, which is an unrealistic condition and hardly realized in real atmosphere, (2) errors introduced by  $\kappa_i$  for individual chemical composition, and (3) the category “others” typically includes organic carbon (OC), elemental carbon (EC), hydrophobic inorganic and other species. Among these other species there are water soluble species contributing to CCN formation. For example, OC has an effective  $\kappa$  value of roughly 0.1 and has been reported to be an important contributor to particle condensational growth. The reasonable closure identified in this study implies that the detailed information of particle size spectra can build an effective CCN prediction model, and size plays a dominant role in aerosol activity during NPF.

It should be noted that the contribution of NPF to CCN has not been fully characterized in this study. For example, the loss of nucleation mode

particles by coagulation and the impact of atmospheric dilution and boundary layer evolution on pre-existing and newly formed CCN are unknown. To fully determine NPF contribution to CCN, additional information on size-resolved aerosol composition, size spectra for 3 nm or smaller particles, atmospheric sink and physicochemical process will be needed.

## **Acknowledgements**

This research is supported by the project of “China Fog-haze monitoring and its numeric forecast operational system at various scales” (2014BAC16B01), the National Natural Science Foundation of China (41475109, 21190053, 21177025, 21277028, 21377029), and partly by the Research and Development Special Fund for Public Welfare Industry (Meteorology) of CMA (GYHY201006047), the Shanghai Science and Technology Commission of Shanghai Municipality (12DJ1400100, 12DZ2260200), the Jiangsu Collaborative Innovation Center for Climate Change, and Priority fields for Ph.D. Programs Foundation of Ministry of Education of China (0110071130003), and the national non-profit scientific research program for environmental protection (201409008).

## **Reference**

Asmi, A., Wiedensohler, A., Laj, P., Fjaeraa, A. M., Sellegri, K., Birmili,

600 W., Weingartner, E., Baltensperger, U., Zdimal, V., Zikova, N., Putaud,  
601 J.-P., Marinoni, A., Tunved, P., Hansson, H.-C., Fiebig, M., Kivekäs, N.,  
602 Lihavainen, H., Asmi, E., Ulevivius, V., Aalto, P. P., Swietlicki, E.,  
603 Kristensson, A., Mihalopoulos, N., Kalivitis, N., Kalapov, I., Kiss, G., de  
604 Leeuw, G., Henzing, B., Harrison, R. M., Beddows, D., O'Dowd, C.,  
605 Jennings, S. G., Flentje, H., Weinhold, K., Meinhardt, F., Ries, L., and  
606 Kulmala, M.: Number size distributions and seasonality of submicro  
607 particles in Europe 2008-2009, *Atmos. Chem. Phys.*, 11, 5505-5538,  
608 doi:10.5194/acp-11-5505-2011, 2011.

609 Benson, D. R., Yu, J. H., Markovich, A., and Lee, S. -H.: Ternary  
610 homogeneous nucleation of  $\text{H}_2\text{SO}_4$ ,  $\text{NH}_3$ , and  $\text{H}_2\text{O}$  under conditions  
611 relevant to the lower troposphere, *Atmos. Chem. Phys.*, 11, 4755-4766,  
612 doi:10.5194/acp-11-4755-2011, 2011.

613 Birmili, W., and Wiedensohler, A.: New particle formation in the  
614 continental boundary layer: meteorological and gas phase parameter  
615 influence, *Geophys. Res. Lett.*, 27, 3325-3328, doi:  
616 10.1029/1999GL011221, 2000.

617 Carslaw, K. S., Spracklen, D. S., Kulmala, M., Kerminen, V. -M., Sihto,  
618 S. L., and Riipinen, I.: The impact of boundary layer nucleation on  
619 global CCN, *Aip. Conf. Proc.*, 911-915, 2007.

620 Cheng, T. T., Han, Z. W., Zhang, R. J., Du, H. H., Jia, X., Wang, J. J., and  
621 Yao, J. Y.: Black carbon in a continental semi-arid area of Northeast

622 China and its possible sources of fire emission, J. Geophys. Res., 115,  
623 D23204, doi: 10.1029/2009JD013523, 2010.

624 Cheng, Y., Lee, S. C., Ho, K. F., Wang, Y. Q., Cao, J. J., Chow, J. C., and  
625 Watson, J. G.: Black carbon measurement in a coastal area of south  
626 China, J. Geophys Res., 111, D12310, doi: 10.1029/2005JD006663,  
627 2006.

628 Dal Maso, M., Kulmala, M., Lehtinen, K. E. J., and Mäkelä, J. M.:  
629 Condensation and coagulation sinks and formation of nucleation mode  
630 particles in coastal and boreal forest boundary layers, J. Geophys. Res.,  
631 107, doi:10.1029/2001JD001053, 2002.

632 Dal Maso, M., Kulmala, M., Riipinen, I., Wagner, R., Hussein, T., Aalto,  
633 P. P., and Lehtinen, K. E. J.: Formation and growth of fresh atmospheric  
634 aerosols: eight years of aerosol size distribution data from SMEAR II,  
635 Hyytiälä, Finland, Boreal Env. Res., 10, 323-336, 2005.

636 Dal Maso, M., Sogacheva, L., Aalto, P. P., Riipinen, I., Komppula, M.,  
637 Tunved, P., Korhonen, L., Suur-Uski, V., Hirsikko, A., Kurtén, T.,  
638 Kerminen, V. -M., Lihavainen, H., Viisanen, Y., Hansson, H. -C., and  
639 Kulmala, M.: Aerosol size distribution measurements at four Nordic  
640 field stations: identification, analysis and trajectory analysis of new  
641 particle formation bursts, Tellus, 59B, 350-361, 2007.

642 Draxler, R. R., and Rolph, G. D.: HYSPLIT (Hybrid Single-Particle  
643 Lagrangian Integrated Trajectory) Model access via NOAA ARL

644 READY Website (<http://www.arl.noaa.gov/HYSPLIT.php>), NOAA Air  
645 Resources Laboratory, Silver Spring, MD, 2014.

646 Du, H. H., Kong, L. D., Cheng, T. T., Chen, J. M., Du, J. F., Li, L., Xia,  
647 X., Leng, C. P., and Huang, G. H.: Insights into summertime haze  
648 pollution events over Shanghai based on online water-soluble ionic  
649 composition of aerosols, *Atmos. Environ.*, 45, 5131-5137, 2011.

650 Du, J. F., Cheng, T. T., Zhang, M., Chen, J. M., He, Q. S., Wang, X. M.,  
651 Zhang, R. J., Tao, J., Huang, G. H., Li, X., and Zha, S. P.: Aerosol size  
652 spectra and particle formation events at urban Shanghai in eastern China,  
653 *Aerosol and Air Quality Research*, 12, 1362-1372, 2012.

654 Dumka, U. C., Krishna Moorthy, K., Kumar, R., Hegde, P., Sagar, R.,  
655 Pant, P., Singh, N., and Suresh Babu, S.: Characteristics of aerosol black  
656 carbon mass concentration over a high altitude location in the Central  
657 Himalayas from multi-year measurements, *Atmos. Res.*, 96, 510-521,  
658 2010.

659 Ehn, M., Thornton, J. A., Kleist, E., Sipilä, M., Juuninen, H., Pullinen, L.,  
660 Springer, M., Rubach, F., Tillmann, R., Lee, B., Lopez-Hilfiker, F.,  
661 Andres, S., Acir, I. H., Rissanen, M., Jokinen, T., Schobesberger, S.,  
662 Kangasluoma, J., Kontkanen, J., Nieminen, T., Kurtén, T., Nielsen, L. B.,  
663 Jørgensen, S., Kjaergaard, H. G., Canagaratna, M., Maso, M. D., Berndt,  
664 T., Petäjä, T., Wahner, A., Kerminen, V. -M., Kulmala, M., Worsnop, D.  
665 R., Wildt, J., and Mentel., T. F.: A large source of low-volatility

666 secondary organic aerosol, *Nature*, 506, 476-479, 2014.

667 Fuchs, N. A. and Sutugin, A. G.: High-dispersed aerosols in *Topics in*  
668 *Current Aerosol Research*, edited by: Hidy, G. M. and Brock, J. R.,  
669 Pergamon, Oxford, 2, 1-60, 1971.

670 Gao, J., Chai, F. H., Wang, T., Wang, S. L., and Wang, W. X.: Particle  
671 number size distribution and new particle formation: New characteristics  
672 during the special pollution control period in Beijing, *J. Environ. Sci.*,  
673 24, 14-21, 2012.

674 Gaydos, T. M., Stanier, C. O., and Pandis, S. N.: Modeling of in situ  
675 ultrafine atmospheric particle formation in the eastern United States, *J.*  
676 *Geophys. Res.*, 110 (D7), doi: 10.1029/2004JD004683, 2005.

677 Ghan, S. J., Easter, R. C., Chapman, E. G., Abdul-Razzak, H., Zhang, Y.,  
678 Leung, L. R., Laulainen, N. S., Saylor, R. D., and Zaveri, R. A.: A  
679 physically based estimate of radiative forcing by anthropogenic sulfate  
680 aerosol, *J. Geophys. Res.*, 106, 5279-5293, 2001.

681 Gong, Y. G., Hu, M., Cheng, Y. F., Su, H., Yue, D. L., Liu, F.,  
682 Wiedensohler, A., Wang, Z. B., Kalesse, H., Liu, S., Wu, Z. J., Xiao, K.  
683 T., Mi, P. C., and Zhang, Y. H.: Competition of coagulation sink and  
684 source rate: New particle formation in the Pearl River Delta of China,  
685 *Atmos. Environ.*, 44, 3278-3285, 2010.

686 Hansen, A. D. A., H. Rosen, and T. Novakov.: The aethalometer-an  
687 instrument for the real-time measurement of optical absorption by

688 aerosol particles, *Sci. Total Environ.*, 36, 191-196, 1984.

689 Hennigan, C. J., Westervelt, D. M., Riipinen, I., Engelhart, G. J., Lee, T.,  
690 Collett, J. L., Pandis, S. N., Adams, P. J., and Robinson, A. L.: New  
691 particle formation and growth in biomass burning plumes: An important  
692 source of cloud condensation nuclei, *Geophys. Res. Lett.*, 39, L09805,  
693 doi: 10.1029/2012GL050930, 2012.

694 Hildebrandt, R. L., Smith, J., Riipinen, I., Barsanti, K., Fry, J., Yli-Juuti,  
695 T., Petaja, T., Kulmala, M., and McMurry, P. H.: The role of nitrate in  
696 the formation of atmospheric nanoparticles: insights from ambient  
697 measurements and chemical transport models, (611f) Environmental  
698 division, American Institute of Chemical Engineers Annual Meeting,  
699 Pittsburgh, PA, 1 November 2012, 2012.

700 Huang, Y. L., Li, L., Li, J. Y., Wang, X., Chen, H., Chen, J. M., Yang, X.,  
701 Cross, D. S., Wang, H., Qiao, L. P., and Chen, H.: A case study of the  
702 highly time-resolved evolution of aerosol chemical and optical  
703 properties in urban Shanghai, China, *Atmos. Chem. Phys.*, 13,  
704 3931-3944, doi:10.5194/acp-13-3931-2013, 2013.

705 Hudson, J. G., and Noble, S.: CCN and vertical velocity influences on  
706 droplet concentrations and supersaturations in clean and polluted stratus  
707 clouds, *J. Atmos. Sci.*, 106, 24119-24126, 2014.

708 Hussein, T., Martikainen, J., Junninen, H., Sogacheva, L., Wagner, R.,  
709 Dal Maso, M., Riipinen, I., Aalto, P. P., and Kulmala, M.: Observation



of regional new particle formation in the urban atmosphere, *Tellus B*, 60, 609-521, doi:10.1111/j.1600-0889.2008.00365.x, 2008.

IPCC: Climate Change 2013: The Physical Science Basis. Contribution of Working Group I to the Fifth Assessment Report of the Intergovernmental Panel on Climate Change, edited by: Jousaume, S., Penner, J., and Tangang, F., IPCC, Stockholm, 2013.

Kerminen, V. -M.: How significantly does coagulation scavenging limit atmospheric particle production?, *J. Geophys. Res.*, 106, 24119-24126, 2001.

Kerminen, V. -M., Lihabainen, H., Lomppula, M., Viisanen, Y., and Kulmala, M.: Direct observational evidence linking atmospheric aerosol formation and cloud droplet activation, *Geophys. Res. Lett.*, 32, L14803, doi: 10.1029/2005GL023130, 2005.

Kerminen, V. -M., Paramonov, M., Anttila, T., Riipinen, I., Fountoukis, C., Korhonen, C., Asmi, E., Laakso, L., Lihavainen, H., Swietlicki, E., Svenningsson, B., Asmi, A., Pandis, S. N., Kulmala, M., and Petäjä, T.: Cloud condensation nuclei production associated with atmospheric nucleation: a synthesis based on existing literature and new results, *Atmos. Chem. Phys.*, 12, 12037-12059, doi:10.5194/acp-12-12037-2012, 2012.

Köhler, H.: The nucleus in and the the growth of hygroscopic droplets, *T. Faraday Soc.*, 32, 1152-1161, 1936.

Kristensson, A., Dal Maso, M., Swietlicki, E., Hussein, T., Zhou, J.,  
Kerminen, V. -M, and Kulmala, M.: Characterization of new particle  
formation events at a background site in Southern Sweden: relation to  
air mass history, *Tellus* 60B, 330-344,  
doi:10.1111/j.1600-0889.2008.00345.x, 2008.

Kulmala, M., Dal Maso, M., Mäkelä, J. M., Pirjola, L., Väkevä, M., Aalto,  
P., Miikkulainen, P., Hämeri, K., and O'Dowd, C. D.: On the formation,  
growth and composition of nucleation mode particles, *Tellus B*, 53,  
479-490, 2001.

Kulmala, M., Laakso, L., Lehtinen, K. E. J., Riipinen, I., Dal Maso, M.,  
Anttila, T., Kerminen, V. -M., Hörrak, U., Vana, M., and Tammet, H.:  
Initial steps of aerosol growth, *Atmos. Chem. Phys.*, 4, 2553-2560,  
doi:10.5194/acp-4-2553-2004, 2004.

Kulmala, M., Petäjä, T., Mönkkönen, P., Koponen, I. K., Dal Maso, M.,  
Aalto, P. P., Lehtinen, K. E. J., and Kerminen, V. -M.: On the growth of  
nucleation mode particles: source rates of condensable vapor in polluted  
and clean environments, *Atmos. Chem. Phys.*, 5, 409-416,  
doi:10.5194/acp-5-409-2005, 2005.

Kulmala, M., Kontkanen, J., Junninen, H., Lehtipalo, K., Manninen, H. E.,  
Nieminen, T., Petäjä, T., Sipilä, M., Schobesberger, S., Rantala, P.,  
Franchin, A., Jokinen, T., Järvinen, E., Äijälä, M., Kangasluoma, J.,  
Hakala, J., Aalto, P. P., Paasonen, P., Mikkilä, J., Vanhanen, J., Aalto, J.,

754 Hakola, H., Aakkonen, U., Ruuskanen, T., Mauldin III, R. L., Duplissy,  
 755 J., Vehkamäki, H., Bäck, J., Kortelainen, A., Riipinen, L., Kurtén, T.,  
 756 Johnston, M. V., Smith, J. N., Ehn, M., Mentel, T. F., Lehtinen, K. E. J.,  
 757 Laaksonen, A., Kerminen, V. -M., and Worsnop, D. R.: Direct  
 758 observations of atmospheric aerosol nucleation, *Science*, 339, 943-946,  
 759 2013.

760 Kulmala, M., Petäjä T., Nieminen, T., Sipilä M., Manninen, H. E.,  
 761 Lehtipato, K., Dal Maso, M., Aalto, P. P., Junninen, H., Paasonen, P.,  
 762 Riipinen, I., Lehtinen, K. E., Laaksonen, A., and Kerminen, V. -M.:  
 763 Measurement of the nucleation of atmospheric aerosol particles, *Nat.*  
 764 *Protoc.*, 7, 1651–1667, 2012.

765 Kuwata, M. and Kondo, Y.: Dependence of size-resolved CCN spectra on  
 766 the mixing state of nonvolatile cores observed in Tokyo. *J. Geophys.*  
 767 *Res.*, 113, D19202, doi: 10.1029/2007JD009761, 2008.

768 Laakso, L., Merikanto, J., Vakkari, V., Laakso, H., Kulmala, M., Molefe,  
 769 M., Kgabi, N., Mabaso, D., Carslaw, K. S., Spracklen, D. V., Lee, L. A.,  
 770 Reddington, C. L., and Kerminen, V. -M.: Boundary layer nucleation as  
 771 a source of new CCN in savannah environment, *Atmos. Chem. Phys*, 13,  
 772 1957-1972, doi:10.5194/acp-13-1957-2013, 2013.

773 Laaksonen, A., Hamed, A., Joutsensaari, J., Hiltunen, L., Cavalli, F.,  
 774 Junkermann, W., Asmi, A., Fuzzi, S., and Facchini, M. C.: Cloud  
 775 condensation nucleus production from nucleation events at a highly

776 polluted region, *Geophys. Res. Lett.*, 32, L06812, doi;  
 777 10.1029/2004GL022092, 2005.

778 Lance, S., Medina, J., Smith, J. N., and Nenes, A.: Mapping the operation  
 779 of the DMT Continuous Flow CCN counter, *Aerosol Sci. Tech.*, 40,  
 780 242-254, 2006.

781 Leng, C. P., Cheng, T. T., Chen, J. M., Zhang, R. J., Tao, J., Huang, G. H.,  
 782 Zha, S. P., Zhang, M. G., Fang, W., Li, X., and Li, L.: Measurements of  
 783 surface cloud condensation nuclei and aerosol activity in downtown  
 784 Shanghai, *Atmos. Environ.*, 69, 354-361, 2013.

785 Lihavainen, H., Kerminen, V. -M., Komppula, M., Hatakka, J., Aaltonen,  
 786 V., Kulmala, M., and Viisanen, Y.: Production of “potential” cloud  
 787 condensation nuclei associated with atmospheric new particle formation  
 788 in north Finland, *J. Geophys. Res.*, 108, D24, 4872, doi;  
 789 10.1029/2003JD003887, 2003.

790 Lohmann, U. and Feichter, J.: Global indirect aerosol effect; a review,  
 791 *Atmos. Chem. Phys.*, 5, 715-737, doi:10.5194/acp-5-715-2005, 2005.

792 McMurry, P. H., Takano, H., and Anderson, G. R.: Study of the ammonia  
 793 (gas)-sulphuric acid (aerosol) reaction rate, *Enviro. Sci. and Tech*, 17,  
 794 347-352, 1983.

795 McMurry, P. H., Fink, M., Sakurai, H., Stolzenburg, M. R., Mauldin, R.  
 796 L., Smith, J., Eisele, F., Moore, K., Sjostedt, S., Tanner, D., Huey, L. G.,  
 797 Nowak, J. B., Edgerton, E., and Voisin, D.: A criterion for new particle

798 formation in the sulfur-rich Atlanta atmosphere, *J. Geophys. Res.*, 110,  
799 D22S02, doi; 10.1029/2005JD005907, 2005.

800 Merikanto, J., Sprackken, D. V., Mann, G. W., Pickering, S. J and Carslaw,  
801 K. S.: Impact of nucleation on global CCN, *Atmos. Chem. Phys.*, 9(21),  
802 8601-8616, doi:10.5194/acp-9-8601-2009, 2009.

803 Metzger, A., Verheggen, B., Dommen, J., Duplissy, J., Prevot, A. S.,  
804 Weingartner, E., Riipinen, I., Kulmala, M., Spracklen, D. V., Carslaw, K.  
805 S., and Baltensperger, U.: Evidence for the role of organic in aerosol  
806 particle formation under atmospheric conditions, *P. Natl. Acad. Sci.*  
807 USA, 107, 6646-6651, 2010.

808 Mönkkönen, P., Koponen, I. K., Lehtinen, K. E. J., Hämeri, K., Uma, R.,  
809 and Kulmala, M.: Measurement in a highly polluted Asian mega city:  
810 observations of aerosol number size distribution, modal parameters and  
811 nucleation events, *Atmos. Chem. Phys.*, 5, 57-66,  
812 doi:10.5194/acp-5-57-2005, 2005.

813 Nieminen, T., Manninen, H. E., Sihto, S. L., Yli-Juuti, T., Mauldin, R. L.,  
814 Petaja, T., Riipinen, I., Kerminen, V. -M., and Kulmala, M.: Connection  
815 of sulfuric acid to atmospheric nucleation in boreal forest, *Environ. Sci.*  
816 *Technol.*, 43, 4715-4721, 2009.

817 O'Dowd, C. D.: Biogenic coastal aerosol production and its influence on  
818 aerosol radiative properties, *J. Geophys Res.*, 106, 1545-1549, 2001.

819 O'Dowd, C. D., Aalto, P., Hämeri, K., Kulmala, M., and Hoffmann, T.:

820 Atmospheric particles from organic vapors, *Nature*, 416, 497-498, 2002.

821 Paasonen, P., Nieminen, T., Asmi, E., Manninen, H. E., Petäjä, T.,  
822 Plass-Dülmer, C., Flentje, H., Birmili, W., Wiedensahler, A., Hörrak, U.,  
823 Metzger, A., Hamed, A., Laaksonen, A., Facchini, M. C., Kerminen, V.  
824 M., and Kulmala, M.: On the role of sulphuric acid and low-volatility  
825 organic vapors in the initial steps of atmospheric new particle formation,  
826 *Atmos. Chem. Phys.*, 10, 11223-11242, doi:10.5194/acp-10-11223-2010,  
827 2010.

828 Petäjä, T., Mauldin, R. L., Kosciuch, E., McGrath, J., Nieminen, T.,  
829 Paasonen, P., Boy, M., Adamov, A., Kotiaho, T., and Kulmala, M.:  
830 Sulfuric acid and OH concentrations in a boreal forest site, *Atmos.*  
831 *Chem. Phys.*, 9, 7435-7448, doi: 10.5194/acp-9-7435-2009, 2009.

832 Petters, M. D., and Kreidenweis, S. M.: A single parameter representation  
833 of hygroscopic growth and cloud condensation nucleus activity, *Atmos.*  
834 *Chem. Phys.*, 7, 1961-1971, doi:10.5194/acp-7-1961-2007, 2007.

835 Petzold, A., Kopp, C., and Niessner, R.: The dependence of the specific  
836 attenuation cross-section on black carbon mass fraction and particle size,  
837 *Atmos. Environ.*, 31, 661-672, 1997.

838 Pierce, J. R., and Adams, P. J.: Efficiency of cloud condensation nuclei  
839 formation from ultrafine particles, *Atmos. Chem. Phys.*, 7, 1367-1379,  
840 doi:10.5194/acp-7-1367-2007, 2007.

841 Pierce, J. R., and Adams, P. J.: Uncertainty in global CCN concentrations

842 from uncertain aerosol nucleation and primary emission rates, *Atmos.*  
843 *Chem. Phys.*, 9, 1339-1356, doi:10.5194/acp-9-1339-2009, 2009.

844 Ramanathan, V., Crutzen, P. J., Kiehl, J. T., and Rosenfeld, D.: Aerosols,  
845 Climate, and the Hydrological Cycle, *Science*, 294, 2119-2124, 2001.

846 Riipinen, I., Pierce, J. R., Yli-Juuti, T., Nieminen, T., Häkkinen, S., Ehn,  
847 M., Junnunen, H., Lehtipalo, K., Petäjä, T., Slowik, J., Chang, R.,  
848 Shantz, N. C., Abbatt, J., Leaitch, W. R., Kerminen, V. -M., Worsnop, D.  
849 R., Pandis, S. N., Donahue, N. M., and Kulmala, M.: Organic  
850 condensation: a vital link connecting aerosol formation to cloud  
851 condensation nuclei (CCN) concentrations, *Atmos. Chem. Phys.*, 11,  
852 3865-3878, doi:10.5194/acp-11-3865-2011, 2011.

853 Roberts, G. C. and Nenes, A.: A continuous-flow streamwise  
854 thermal-gradient CCN chamber for atmospheric measurements, *Aerosol*  
855 *Sci. Tech.*, 39, 206-221, 2006.

856 Sakurai, T., Fujita, S. I., Hayami, H., and Furuhashi, N.: A study of  
857 atmospheric ammonia by means of modeling analysis in the Kanto  
858 region of Japan, *Atmos. Environ.*, 39, 203-210, 2005.

859 Shen, X. J., Sun, J. Y., Zhang, Y. M., Wehner, B., Nowak, A., Tuch, T.,  
860 Zhang, X. C., Wang, T. T., Zhou, H. G., Zhang, X. L., Dong, F., Birmili,  
861 W., and Wiedensohler, A.: First long-term study of particle number size  
862 distributions and new particle formation events of regional aerosol in the  
863 North China Plain, *Atmos. Chem. Phys.*, 11, 1565-1580,

doi:10.5194/acp-11-1565-2011, 2011.

Smith, J. N., Moore, K. F., McMurry, P. H., and Eisele F. L.: Atmospheric measurements of sub-20 nm diameter particle chemical composition by thermal desorption chemical ionization mass spectrometry, *Aerosol Sci. Technol*, 38, 100-110, 2004.

Spracklen, D. V., Carslaw, K. S., Kulmala, M., Kerminen, V. M., Mann, G. W., and Sihto, S. L.: The contribution of boundary layer nucleation events to total particle concentrations on regional and global scales, *Atmos. Chem. Phys.*, 6, 5631-5648, doi:10.5194-acp-6-5631-2006, 2006.

Spracklen, D. V., Carslaw, K. S., Kulmala, M., Kerminen, V. M., Sihto, S. L., Riipinen, I., Merikanto, J., Mann, g. w., Chipperfield, M. P., Wiedensohler, A., Birmili, W., and Lihavainen, H.: Contribution of particle formation to global cloud condensation nuclei concentrations, *Geophys. Res. Lett.*, 35, L06808, doi:10.1029/2007GL033038, 2008.

Vehkamäki, H., Dal Maso, M., Hussein, T., Flannagan, R., Hyvärinen, A., Lauros, J., Merikanto, J., Mönkkönen, P., Pihlatie, M., Salminen, K., Sogacheva, L., Thum, T., Ruuskanen, T. M., Keronen, P., Aalto, P. P., Hari, P., Lehtinen, K. E. J., Rannik, Ü., and Kulmala, M.: Atmospheric particle formation events at Värriö measurement station in Finnish Lapland 1998-2002, *Atmos. Chem. Phys.*, 4, 2015-2023, doi:10.5194/acp-4-2015-2004, 2004.



886 Vuollekoski, H., Kerminen, V. -M., Anttila, T., Sihto, S. L., Vana, M., Ehn,  
887 M., Korhonen, H., McFiggans, G., O'Dowd, C. D., and Kulmala, M.:  
888 Iodine dioxide nucleation simulations in coastal and remote marine  
889 environments, *J. Geophys. Res.*, 114, D00206, doi:  
890 10.1029/2008JD010713, 2009.

891 Wang, X. F., Zhang, Y. P., Chen, H., Yang, X., and Chen, J. M.: Particle  
892 nitrate formation in a highly polluted urban area: a case study by  
893 single-particle mass spectrometry in Shanghai, *Environ. Sci. Technol.*,  
894 43, 3061-3066, 2009.

895 Wang, Y., Zhuang, G. S., Zhang, X. Y., Huang, K., Xu, C., Tang, A. H.,  
896 Chen, J. M., and An, Z. S.: The ion chemistry, seasonal cycle, and  
897 sources of PM<sub>2.5</sub> TSP aerosol in Shanghai, *Atmos. Environ.*, 40,  
898 2935-2952, 2006.

899 Wang, Z. B., Hu, M., Sun, J. Y., Wu, Z. J., Yue, D. L., Shen, X. J., Zhang,  
900 Y. M., Pei, X. Y., Cheng, Y. F., and Wiedensohler, A.: Characteristics of  
901 regional new particle formation in urban and regional background  
902 environments in the North China Plain, *Atmos. Chem. Phys.*, 13,  
903 12495-12506, 3013.

904 Wang, Z. B., Hu, M., Wu, Z. J., and Yue, D. L., Research on the  
905 formation mechanism of new particles in the atmosphere, *Acta Chim.*  
906 *Sinica*, 71, 519-527, 2013.

907 Weber, R. J., Marti, J. J., McMurry, P. H., Eisele, F. L., Tanner, D. J., and

908 Jefferson, A.: Measured atmospheric new particle formation rates:  
 909 Implications for nucleation mechanisms, *Chem. Eng. Commun.*, 151,  
 910 53-64, 1996.

911 Weber, R. J., McMurry, P. H., Mauldin, R. L., Tanner, D. J., Eisele, F. L.,  
 912 Clarke, A. D., and Kapustin, V. N.: New particle formation in the remote  
 913 troposphere: a comparison of observations at various sites, *Geophys.*  
 914 *Res. Lett.*, 26, 307-310, doi:10.1029/1998GL900308, 1999.

915 Weingartner, E., Saathoff, H., Schnaiter, M., Streit, N., Bitnar, B., and  
 916 Baltensperger, U.: Absorption of light by soot particles: determination of  
 917 the absorption coefficient by means of aethalometers, *J. Aerosol Sci.*, 34,  
 918 1445-1463, 2003.

919 Wiedensohler, A., Cheng, Y. F., Nowak, A., Wehner, B., Achtert, P.,  
 920 Berghof, M., Birmili, W., Wu, Z. J., Hu, M., Zhu, T., Takegawa, N., Kita,  
 921 K., Kondo, Y., Lou, S. R., Hofzumahaus, A., Holland, F., Wahner, A.,  
 922 Gunthe, S. S., Rose, D., Su, H., and Pöschl, U.: Rapid aerosol growth  
 923 and increase of cloud condensation nucleus activity by secondary  
 924 aerosol formation and condensation: a case study for regional air  
 925 pollution in northeastern China, *Geophys. Res. Lett.*, 114, D00G08,  
 926 doi:10.1029/2008JD010884, 2009

927 Wu, Z., Hu, M., Liu, S., Wehner, B., Bauer, S., Määßling, A. Wiedensohler,  
 928 A., Petäjä, T., Dal Maso, M., and Kulmala, M.: New particle formation  
 929 in Beijing, China: statistical analysis of a 1-year dataset, *J. Geophys.*

930 Res., 112, D09209, doi; 10.1029/2006JD007406, 2007.

931 Wu, Z. J., Hu, M., Lin, P., Liu, S., Wehner, B., and Wiedensohler, A.:  
932 Particle number size distribution in the urban atmosphere of Beijing,  
933 China, Atmos. Environ., 42, 7967-7980,  
934 doi:10.1016/j.atmosenv.2008.06.022, 2008.

935 Yu, F. Q.: Effect of ammonia on new particle formation: a kinetic  
936  $\text{H}_2\text{SO}_4\text{-H}_2\text{O-NH}_3$  nucleation model constrained by laboratory  
937 measurements, J. Geophys. Res., 111, D01204, doi;  
938 10.1029/2005JD005968, 2006.

939 Yu, F., Wang, Z., Luo, G., and Turco, R.: Ion-mediated nucleation as an  
940 important global source of tropospheric aerosols, Atmos. Chem. Phys., 8,  
941 2537-2554, doi:10.5194/acp-8-2537-2008, 2008.

942 Yu, H., McGraw, R., and Lee, S. H.: Effects of amines on formation of  
943 sub-3 nm particles and their subsequent growth, Geophys. Res. Lett., 39,  
944 L02807, doi: 10.1029/2011GL050099, 2012.

945 Yue. D. L., Hu. M., Zhang. R. J., Wu. Z. J., Su. H., Wang, Z. B., Peng, J.  
946 F., He, L. Y., Huang, X. F., Gong, Y. G., and Wiedensohler, A.: Potential  
947 contribution of new particle formation to cloud condensation nuclei in  
948 Beijing, Atmos. Environ., 45, 6070-6077, 2011.

949 Zhang, R. J., Jing, J. S., Tao, J., Hsu, S.-C., Wang, G., Cao, J. J., Lee, C. S.  
950 L., Zhu, L., Chen, Z., Zhao, Y., and Shen, Z.: Chemical characterization  
951 and source apportionment of  $\text{PM}_{2.5}$  in Beijing: seasonal perspective,

Atmos. Chem. Phys., 13, 7053-7074, doi:10.5194/acp-13-7053-2013,  
2013.

Zhang, R. Y.: Getting to the critical nucleus of aerosol formation, Science,  
328, 1366-1367, 2010.

Zhang, R. Y., Khalizov, A., Wang, L., Hu, M., and Xu, W.: Nucleation  
and growth of nanoparticles in the atmosphere, Chem. Rev., 112,  
1957-2011, 2012.

Zheng, J., Hu, M., Zhang, R., Yue, D., Wang, Z., Guo, S., Li, X., Bohn, B.,  
Shao, M., He, L., Huang, X., Wiedensohler, A., and Zhu, T.:  
Measurements of gaseous H<sub>2</sub>SO<sub>4</sub> by AP-ID-CIMS during CAREBijng  
2008 Campaign, Atmos. Chem. Phys., 11, 7755-7765,  
doi:10.5194/acp-11-7755-2011, 2011.

**Table 1.** Comparison of CCN enhancement ratios from NPF events with different formation and growth rates.

	0.2%	0.4%	0.6%	0.8%	1.0%
Enhancement ratio (FR>0.40)	1.18	1.84	1.88	1.84	1.77
Enhancement ratio (FR<0.40)	1.15	1.89	1.81	1.77	1.58
Enhancement ratio (GR>4.91)	1.25	1.95	2.03	1.93	1.72
Enhancement ratio (GR<4.91)	1.10	1.79	1.80	1.74	1.63

**Table 2.** Effective hygroscopicity parameters ( $\kappa$ ) and densities of the four category compositions.

Species	Data source	$\kappa$	Density (g cm <sup>-3</sup> )
Sulfate & nitrate	SO <sub>4</sub> <sup>2-</sup> +NO <sub>3</sub> <sup>-</sup> +NH <sub>4</sub> <sup>+</sup>	0.6	1.7
Sodium chloride	Cl <sup>-</sup> +Na <sup>+</sup>	1	2.2
Insoluble compounds	Others	0	2.0

## Figure captions

**Figure 1.** Series of 10-min mean meteorological parameters over the entire campaign.

**Figure 2.** Series of 5-min mean SO<sub>2</sub> and PM<sub>2.5</sub> concentration and atmospheric visibility over the entire campaign.

**Figure 3.** Series of aerosol size distribution, 4-min mean total (N<sub>total</sub>) and nucleation (N<sub>10-20nm</sub>) mode aerosol number concentration and 1-hour mean CCN concentration over the entire campaign.

**Figure 4.** Temporal evolution of 4-min mean aerosol size spectra, showing new particle formation and subsequent growth on 3 and 4 April 2012.

**Figure 5.** Temporal evolution of 10-min mean meteorological parameters during the new particle formation event on 3-4 April 2012.

**Figure 6.** Temporal evolutions of 5-min mean atmospheric visibility, BC and PM<sub>2.5</sub> concentrations during the new particle formation event on 3-4 April 2012.

**Figure 7.** Temporal evolutions of 4-min mean mode, median and diameters and 10-20 nm particle concentration, showing the growth rate and formation of new particle on 3-4 April 20.

**Figure 8.** Series of 1-h mean SO<sub>2</sub>, SO<sub>4</sub><sup>2-</sup>, NO<sub>3</sub><sup>-</sup> and NH<sub>4</sub><sup>+</sup> concentrations on 3 and 4 April 2012.

**Figure 9.** Series of 1-h mean CCN concentration and CCN/CN on 3 and 4 April 2012.

**Figure 10.** Scatterplots of predicted and measured CCN concentrations at different SS conditions, the red dash line represents y=x.

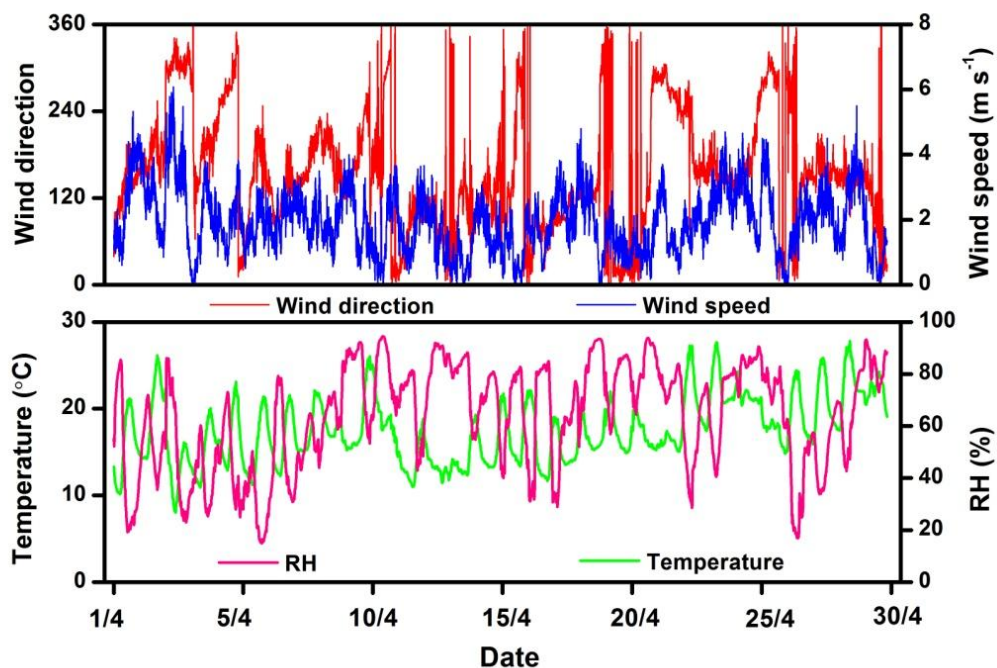


Figure 1. Series of 10-min mean meteorological parameters over the entire campaign.

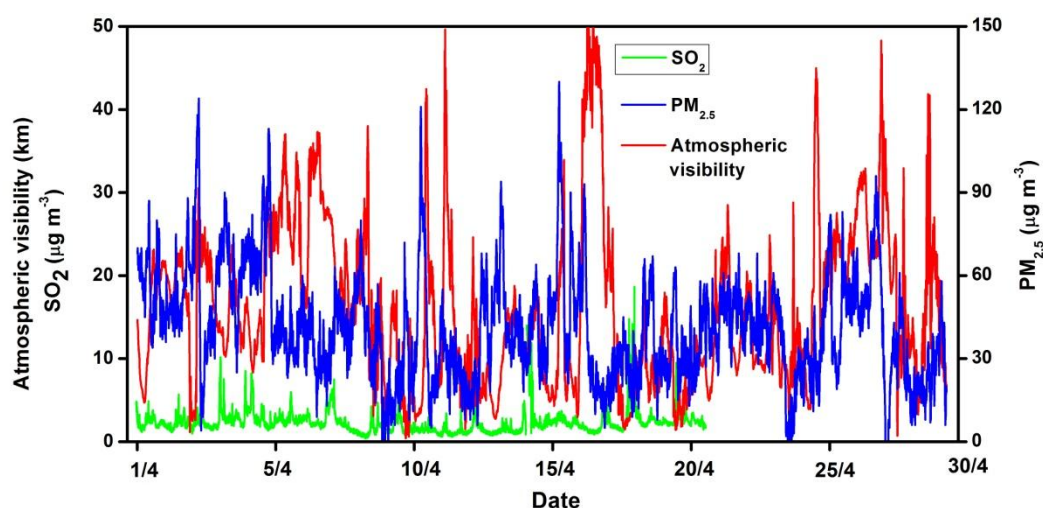


Figure 2. Series of 5-min mean  $\text{SO}_2$  and  $\text{PM}_{2.5}$  concentration and atmospheric visibility over the entire campaign.

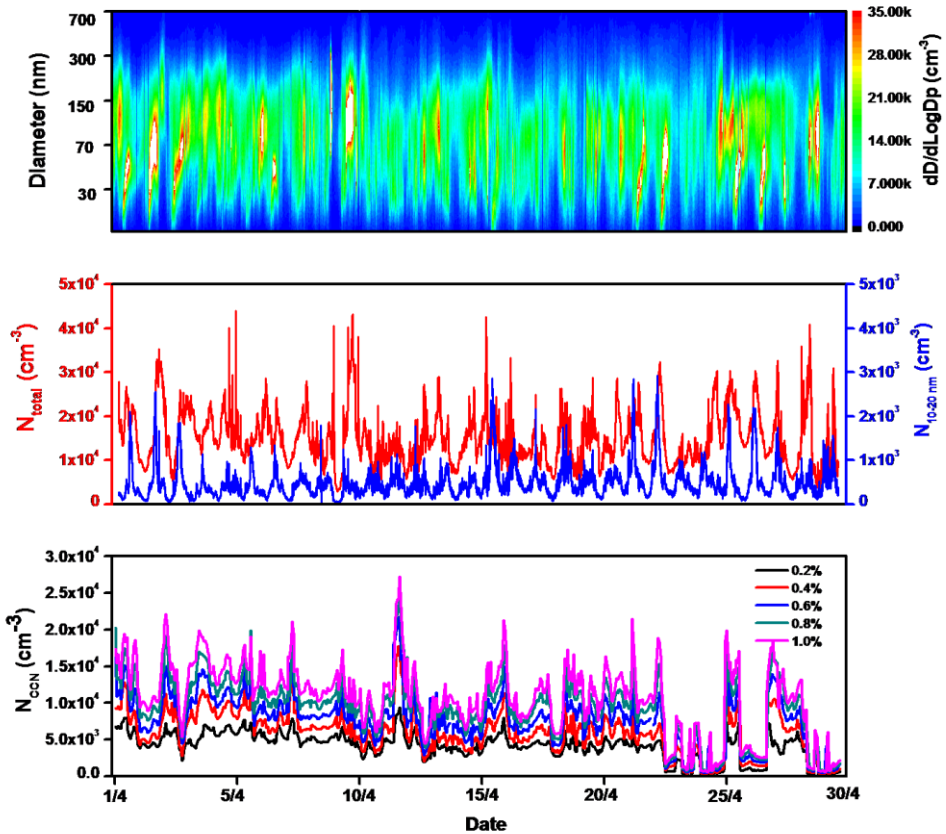


Figure 3. Series of aerosol size distribution, 4-min mean total ( $N_{total}$ ) and nucleation ( $N_{10-20nm}$ ) mode aerosol number concentration and 1-hour mean CCN concentration over the entire campaign.

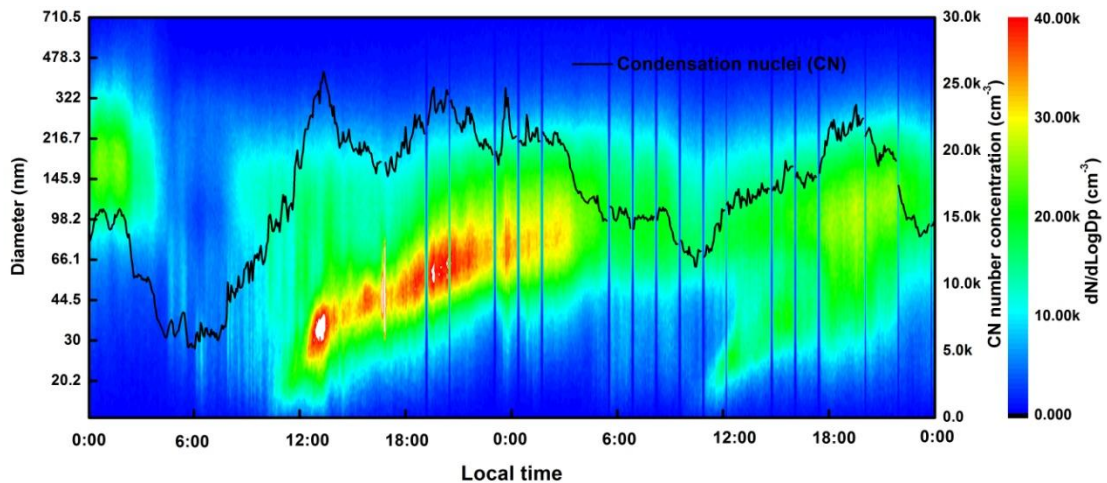


Figure 4. Temporal evolution of 4-min mean aerosol size spectra, showing new particle formation and subsequent growth on 3 and 4 April 2012.



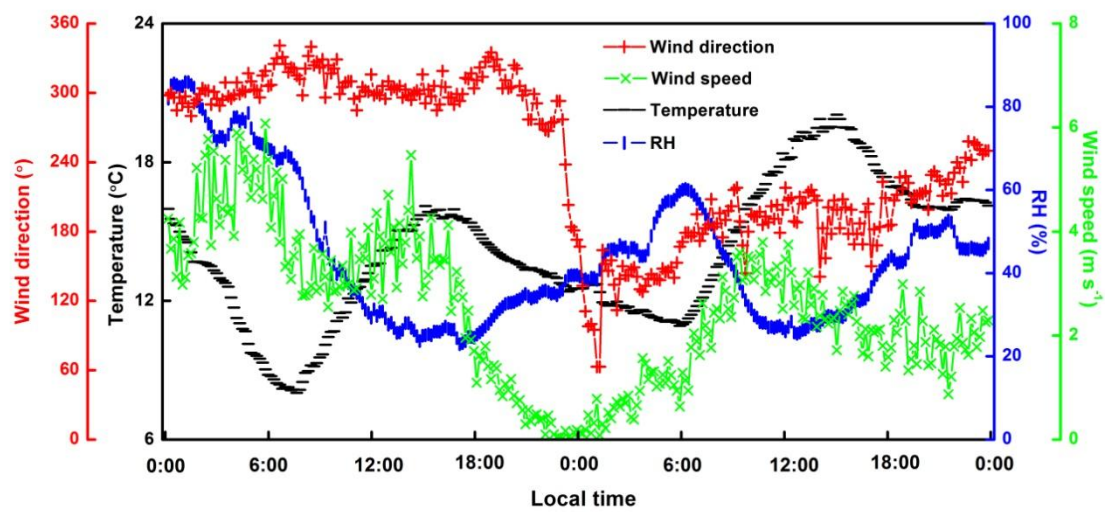


Figure 5. Temporal evolution of 10-min mean meteorological parameters during the new particle formation event on 3-4 April 2012.

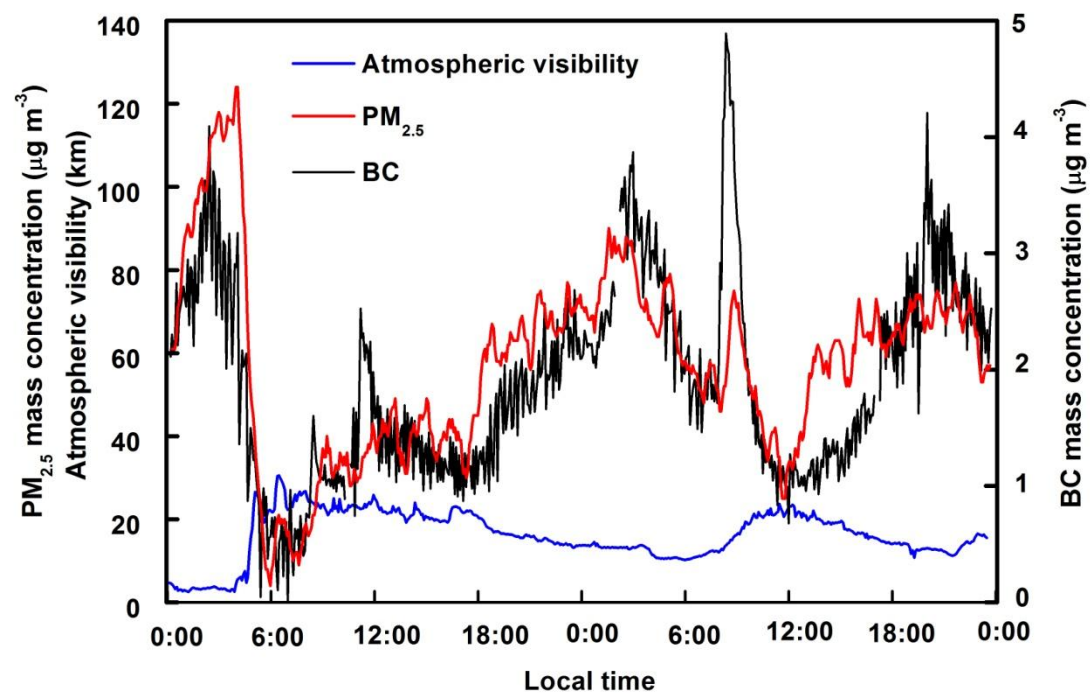


Figure 6. Temporal evolutions of 5-min mean atmospheric visibility, BC and  $PM_{2.5}$  concentrations during the new particle formation event on 3-4 April 2012.

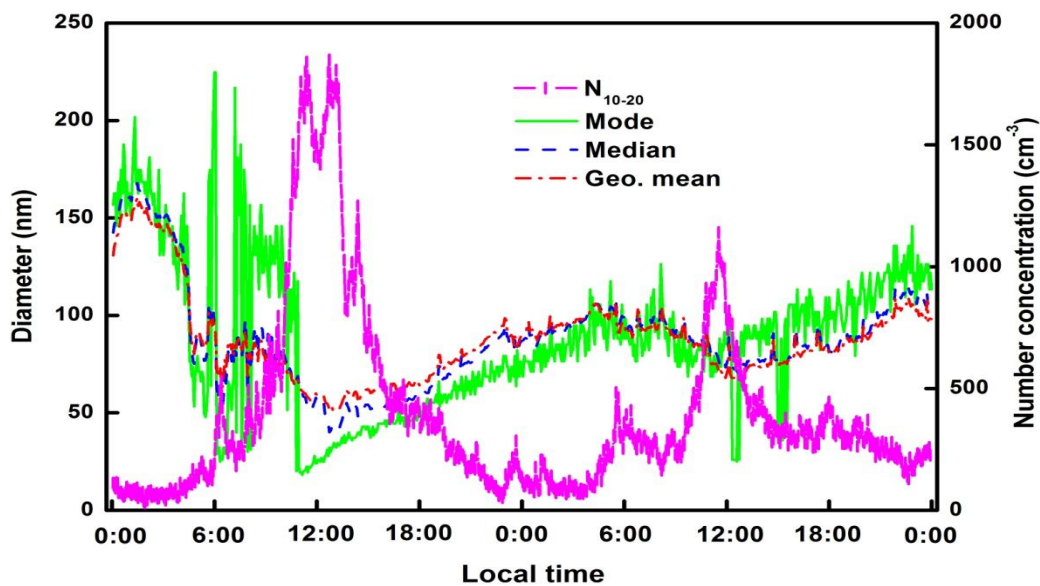


Figure 7. Temporal evolutions of 4-min mean mode, median and diameters and 10-20 nm particle concentration, showing the growth rate and formation of new particle on 3-4 April 20.

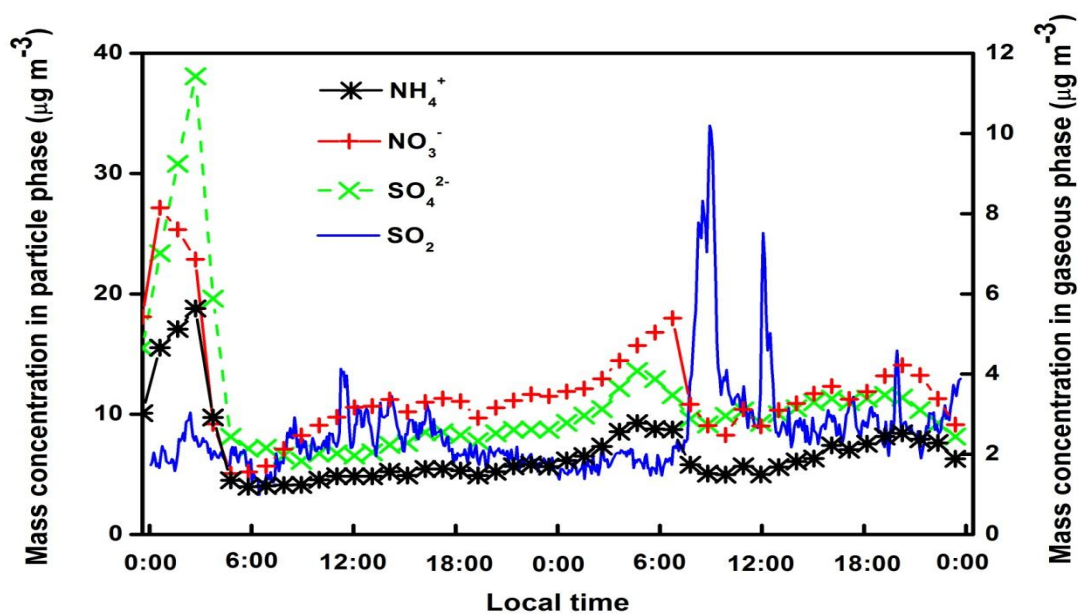


Figure 8. Series of 1-h mean  $\text{SO}_2$ ,  $\text{SO}_4^{2-}$ ,  $\text{NO}_3^-$  and  $\text{NH}_4^+$  concentrations on 3 and 4 April 2012.

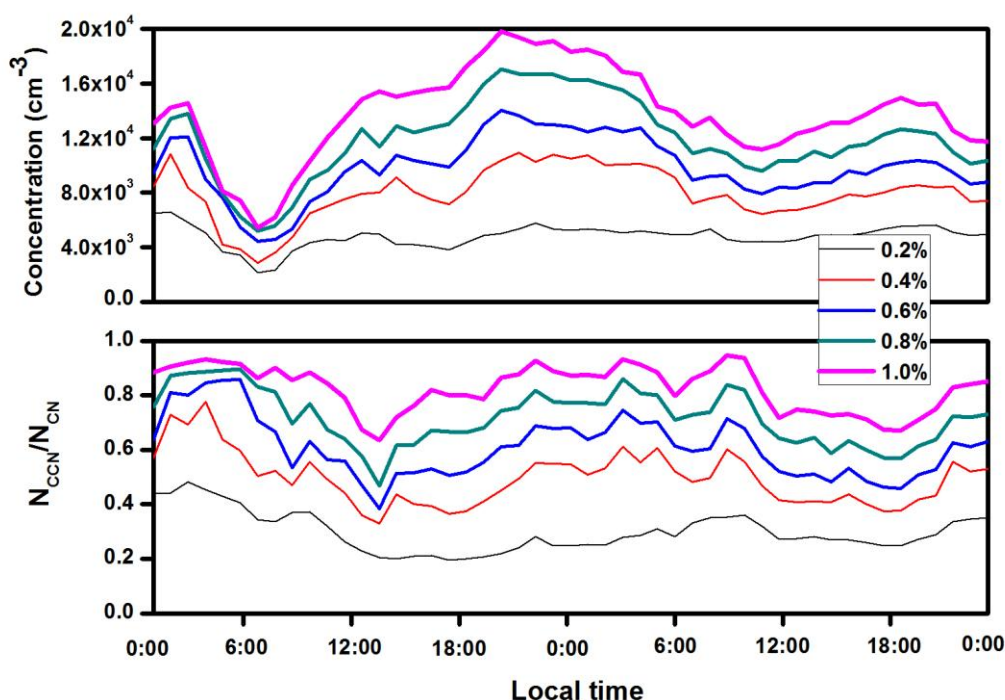


Figure 9. Series of 1-h mean CCN concentration and CCN/CN on 3 and 4 April 2012.

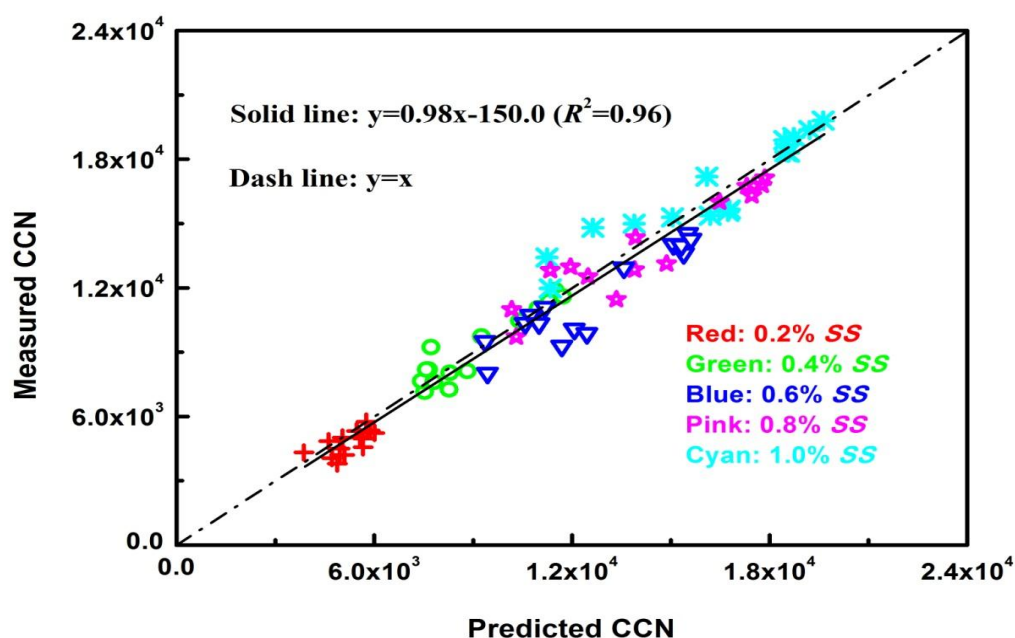


Figure 10. Scatterplots of predicted and measured CCN concentrations at different SS conditions, the red dash line represents  $y = x$ .